Hybridization Framework for Improved Dynamic Phasor Parameter Estimation Algorithms

Cheng Qian, *Graduate Student Member, IEEE*, Mladen Kezunovic, *Life Fellow, IEEE*

Dept. of Electrical and Computer Engineering
Texas A&M University, College Station
College Station, TX, US
peterqiancheng@tamu.edu, kezunov@ece.tamu.edu

***Abstract*—With an increasingly wider application of Phasor Measurement Units (PMUs), the accuracy of phasor parameter estimation has become one of the major concerns in related research. The accuracy of phasor parameter estimation is closely associated with the accuracy of waveform model representation. The most commonly used waveform models in literature are Fourier models, and Taylor polynomial models, which are the backbones of frequency-domain and time-domain phasor estimation approaches, respectively. Usually, neither solution alone is capable of producing satisfactory results, despite various improvement strategies. This paper proposes a novel method for hybridization of existing Fourier and polynomial fitting-based estimation methods. The framework is introduced so that the merits from multiple algorithms can be leveraged without designing a completely new algorithm. Fourier method and Taylor expansion method are selected to demonstrate this approach. Both theoretical derivation and simulation results show that the proposed framework effectively integrates the benefits from both algorithms to achieve sufficient accuracy.**

***Index Terms*—Algorithm hybridization, hybrid method, parameter estimation, phasor measurement, power system measurement**

I. INTRODUCTION

Mostly recently, synchronized phasor measurement technology has gained wide acknowledgement and growing investment, and it has shown its benefits in power system monitoring in both transmission and distribution systems [1]-[7].

Phasor representation describes input waveforms within a short observation window with three parameters: amplitude, phase angle, and frequency. The definition of phasor is well known and in the USA usually assumes 60Hz operating frequency. Dynamic phasors, on the other hand, as a relatively new definition, was proposed in [8], and is recognized in subsequent IEEE standards [9]. Unlike static phasors, dynamic phasor assumes the waveform parameters may change over the length of an observation window. As a result, each time instant in a data window is theoretically associated with a distinct phasor value. Most recently, dynamic phasor modeling is adopted in the calculation of phasor parameters.

Phasor estimation methods are assumed to be associated with a predetermined waveform model with unknown parameters. Phasor parameters are thereafter calculated using the estimated waveform features. Most commonly, phasor parameters can be estimated using Fourier methods. For example, Discrete Fourier Transform (DFT) [10]. Fourier methods interpret input waveform as a linear combination of sinusoidal waves at different frequencies, and each sinusoidal wave is in steady-state, indicating constant amplitude and frequency [11]. As a result, Fourier methods only produce ideal results when the assumed frequency composition fits actual waveform frequency profile. Otherwise, frequency leakage occurs and phasors cannot be accurately estimated [12]. Various efforts, such as interpolated DFT (IpDFT) method are designed to improve traditional DFT method by compensating frequency leakage [13]. Those aforementioned Fourier-based methods are sometimes categorized as "frequency-domain" methods.

The major caveat in Fourier-based methods is the assumption that waveform parameters remain constant during an observation window, which inevitably introduces large error when there are variations in waveform amplitude and frequency. The estimation errors are alleviated by approximating the dynamic features in waveforms using time-domain polynomial expansion [14,15]. This strategy can effectively model slow transients such as amplitude variations, but fails to consider abrupt changes and harmonics.

A model that integrates both slow transients and multifrequency features attempted to solve this problem. This method models harmonic components in Fourier methods using Taylor expansion as well, and therefore, are named "Taylor-Fourier" transforms [16]-[18]. This feasible yet complicated model usually leads to a fairly large size fitting matrix, and therefore, is usually expensive to compute.

In this paper, a novel framework to hybridize the aforementioned Fourier methods and time-domain methods is proposed. The hybridization can effectively integrate the benefits of both Fourier and Taylor expansion methods without significant computational burden.

This work was supported by the US Department of Energy (DoE) project "Timing Intrusion Management Ensuring Resiliency (TIMER)".

The rest of the paper is organized as follows. Section II clarifies the problem and gives the framework for algorithm hybridization. Methodology of hybridization is introduction in Section III, where two strategies are introduced. The proposed framework is tested in Section IV, and conclusions are given in Section V.

II. Problem Statement and Proposed Solution

A. Fourier Method and Taylor-Fourier Method Revisited

According to IEEE Standard [10], power system waveform can be expressed in (1):

$$\begin{aligned} x_1(t) &= a(t)\cdot\cos\left[2\pi f_0 t + 2\pi\int \Delta f(t)\,\mathrm{d}t + \phi_0\right] \\ &= a(t)\cdot\cos[2\pi f_0 t + \phi(t)] \end{aligned} \quad (1)$$

where $a(t)$, f_0, ϕ_0, $\Delta f(t)$, $\phi(t)$ denotes instantaneous amplitude, nominal frequency, initial phase angle, instantaneous frequency deviation, and instantaneous phase angle, respectively.

As a common practice in time domain methods [14,15], (1) can be expanded as:

$$x_1(t) = q(t)\cos(2\pi f_0 t\,) + r(t)\sin(2\pi f_0 t\,) \quad (2)$$

where $q(t) \triangleq a(t)\cos[\phi(t)]$, $r(t) \triangleq -a(t)\sin[\phi(t)]$.

Note that (1) reflects the slow variations on f_0 component, represented by $a(t)$ and $\phi(t)$ terms, but does not take into account any harmonic components. This practice is reasonable since harmonic components are not of interested and should always be eliminated.

For the discussion in the paper, (2) is rewritten so that harmonic components are reflected:

$$x(t) = x_1(t) + \sum_{k=2}^{K} h(t;k,\boldsymbol{a}) \quad (3)$$

where $h(k,a;t)$ reflects harmonic terms, k is harmonic order, $\boldsymbol{a}$ is a vector showing the harmonic characteristics, such as amplitude, phase angle, t is time.

One common process to treat $q(t)$ and $r(t)$ in (2) is approximation using polynomials [8], shown in (4):

$$q(t) = \sum_{m=0}^{M-1} c_m P(t;m)\,;\, r(t) = \sum_{m=0}^{M-1} s_m P(t;m) \quad (4)$$

where m is the order of polynomial $P(t;m)$, M is the number of terms in the approximation. Most cases in literature use $M = 3$.

If we rewrite (3), we have:

$$\begin{aligned} x(t) = &\sum_{m=0}^{M-1} c_m P(t;m)\cdot\cos(2\pi f_0 t\,) + \\ &\sum_{m=0}^{M-1} s_m P(t;m)\cdot\sin(2\pi f_0 t\,) + \sum_{k=2}^{K} h(t;k,\boldsymbol{a}) \end{aligned} \quad (5)$$

In polynomial methods, harmonic terms $\sum_{k=2}^{K} h(t;k,\boldsymbol{a})$ are neglected. In DFT-based methods. Typically M is set to 1, resulting in the commonly known spectrum representation. Consequently, polynomial methods are susceptible to harmonic infiltration, whereas DFT-based methods cannot accurately track the slow dynamics in input waveforms.

A hybridization framework is designed to integrate polynomial methods and DFT method so that the resultant algorithm is capable of rejecting harmonics and tracking slow varying transients at the same time. The framework is shown in block diagram as Fig. 1.

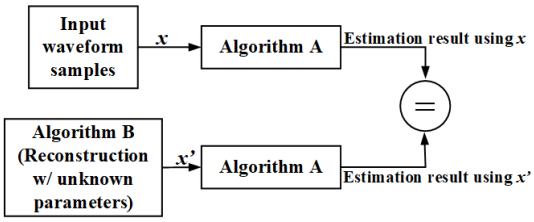

Figure 1. Proposed Hybridization Framework for two Algorithms

Instead of directly estimating phasor parameters, the proposed framework acknowledges that neither algorithm alone will yield satisfactory results. Algorithm A in this framework is leveraged as a filter with which some of the undesired features are removed from the input. The principle is, when the reconstructed waveform x' is a desirable replica of input waveform x, the same output from Algorithm A (filter) should be expected. In this paper, candidate methods from either frequency domain or time domain are selected for a simple demonstration of the proposed framework.

III. Algorithm Hybridization Methodology

In this section, hybridization of DFT [10] and monomial fitting method [8] is demonstrated. In order to demonstrate that the framework is capable of modeling slow varying transients as well as rejecting harmonics, the "true" input waveform in (3) is rewritten as:

$$x(\boldsymbol{t}) = f(\boldsymbol{t}) + h(\boldsymbol{t}) \quad (6)$$

where bold font represents vector, $\boldsymbol{t}$ represents time, $f(\boldsymbol{t})$ is the sinusoidal waveform with varying envelope, modeled with (2), $h(\boldsymbol{t})$ is the harmonic term.

A. Monomial Fitting Method is Used for Reconstruction

In monomial fitting method [8], $P(t;m) = t^m$, $m = 0,1,2$. Expanding input waveform at the center of observation window, the reconstructed waveform can be expressed as:

$$x'(\boldsymbol{t}) \coloneqq H\boldsymbol{c} \quad (7)$$

where,

$$\begin{aligned} H &= [\boldsymbol{\gamma_0}, \boldsymbol{\delta_0}, \boldsymbol{\gamma_1}, \boldsymbol{\delta_1}, \boldsymbol{\gamma_2}, \boldsymbol{\delta_2}] \\ \boldsymbol{\gamma_i} &\coloneqq (\boldsymbol{t} - t_c)^i \cdot \cos(2\pi f_0 \boldsymbol{t}) \\ \boldsymbol{\delta_i} &\coloneqq -(\boldsymbol{t} - t_c)^i \cdot \sin(2\pi f_0 \boldsymbol{t}) \\ \boldsymbol{c} &\coloneqq [c_0, s_0, c_1, s_1, c_2, s_2]^T \end{aligned} \quad (8)$$

where t_c represents the center of observation window, $(*)^T$ is transpose operation.

Monomial fitting method represented in (7) and (8) captures the slow varying dynamics in waveform envelopes with high accuracy, and therefore, we may assume $f(\boldsymbol{t}) \equiv x'(\boldsymbol{t}) = H\boldsymbol{c}$ with acceptable fitting error. On the other hand, $h(\boldsymbol{t})$ term can be filtered out using Algorithm A (DFT in this case). Therefore, if waveform $x'(\boldsymbol{t})$ contains all the desired information in a particular application, using Algorithm A to filter either waveform $x(\boldsymbol{t})$ or waveform $x'(\boldsymbol{t})$ should yield the same results.

For Algorithm A, DFT calculation can be defined by: $X(\boldsymbol{k}) = Wx(\boldsymbol{t})$, where $X(k)$ is the kth harmonic component, W is the DFT matrix, defined as: $W_{m,n} = \frac{1}{\sqrt{N}}\omega^{mn}$, where $m,n = 0,1,2,\ldots,N\text{-}1$, $j \equiv \sqrt{-1}$, $\omega \equiv e^{-j2\pi/N}$, N is the number of samples in an observation window.

From the mathematical expression, it can be seen that each row of matrix W extracts one frequency component from input waveform. Due to the restriction of Nyquist theorem, up to half the sampling frequency can be extracted, the positive and negative images are actually complex conjugate pairs. Matrix W can be rearranged as shown in (9):

$$W = \begin{bmatrix} A \\ W' \end{bmatrix}$$
$$A = \frac{1}{\sqrt{N}}\begin{bmatrix} 1 & \omega^{p} & \omega^{2p} & \cdots & \omega^{(N-1)p} \\ 1 & \omega^{N-p} & \omega^{2(N-p)} & \cdots & \omega^{(N-1)(N-p)} \end{bmatrix} \quad (9)$$

where p is the number of nominal cycles in an observation window. Since the only frequency components of interest are ±60Hz (depending on the length of observation window, ±60Hz may corresponds to particular harmonics), only two rows associated with ±60Hz of matrix W are used, stored in A.

Applying Fourier analysis W on $x(\boldsymbol{t})$:

$$Wx(\boldsymbol{t}) = \begin{bmatrix} A \\ W' \end{bmatrix}[f(\boldsymbol{t}) + h(\boldsymbol{t})] = \begin{bmatrix} Af(\boldsymbol{t}) + Ah(\boldsymbol{t}) \\ W'f(\boldsymbol{t}) + W'h(\boldsymbol{t}) \end{bmatrix} \quad (10)$$

The expression $Ax(\boldsymbol{t})=Af(\boldsymbol{t})+Ah(\boldsymbol{t})$ yields the Fourier spectrum components of ±60Hz, which are in fact, complex conjugate. Since $h(\boldsymbol{t})$ does not contain any ±60Hz components, $Ah(\boldsymbol{t})\equiv 0$. For the sake of simplicity, only ±60Hz component will be analyzed. As a result, matrix A instead of W is used for Fourier analysis.

As discussed before, Fourier analysis is performed on both the original waveform $x(\boldsymbol{t})$ and the reconstructed waveform $x'(\boldsymbol{t})$, and the results should be the same when reconstruction is assumed to be accurate. Thus, the following simple identity holds.

$$Ax'(\boldsymbol{t}) = AH\boldsymbol{c} \cong Ax(\boldsymbol{t}) = Af(\boldsymbol{t}) \coloneqq \boldsymbol{b} \quad (11)$$

where A is the DFT matrix extracting real and imaginary parts of ±60Hz components, H is defined in (7) and (8), $\boldsymbol{x}$ is input waveform sample vector, $\boldsymbol{b}$ is the equivalent real and imaginary parts of ±60Hz complex conjugate components, $\boldsymbol{c}$ is the unknown vector of interest.

Eq. (11) is the theoretical justification of proposed hybrid method where DFT is essentially used to reject harmonics. The same logic can also be applied when DFT is used as reconstruction function, as discussed in the following section.

B. DFT is Used for Reconstruction

It should be noted that DFT is a curve fitting method as well, where the basis vectors are in fact harmonic components. Therefore, the formulation of this scheme should be essentially the same as in Section A.

Consider reconstructed waveform $x'(\boldsymbol{t})$ with three frequency components, shown in (12):

$$x'(\boldsymbol{t}) \coloneqq M\boldsymbol{c} \quad (12)$$

where,

$$M = [\boldsymbol{m_0}, \boldsymbol{n_0}, \boldsymbol{m_1}, \boldsymbol{n_1}, \boldsymbol{m_2}, \boldsymbol{n_2}]$$
$$\boldsymbol{m_i} \coloneqq \cos(2\pi f_i \boldsymbol{t})$$
$$\boldsymbol{n_i} \coloneqq -\sin(2\pi f_i \boldsymbol{t}) \quad (13)$$
$$\boldsymbol{c} \coloneqq [c_0, s_0, c_1, s_1, c_2, s_2]^T$$

where f_i are pre-selected frequencies that can be the output of spectrum analysis of input waveform. The case of three frequency components are selected here as an example. Polynomial fitting method in (8) is used as the filtering algorithm.

Similarly, we have:

$$\boldsymbol{d} \coloneqq H^{+}x(\boldsymbol{t}) \cong H^{+}M\boldsymbol{c} \quad (14)$$

where $(H)^{+}\coloneqq(H^{T}H)^{-1}H^{T}$ denotes pseudo-inverse. Note that the column space of H is incomplete, since limited terms are used for expansion.

To demonstrate how to improve the accuracy of (14), an analogous example in three-dimension is illustrated, shown in Fig. 2. Assume vector $\boldsymbol{a}$ (blue arrow) is the "true" waveform vector in 3-D, which is practically observed and thus approximated in 2-D space $\mathcal{S}$=span$\{\boldsymbol{i},\boldsymbol{j}\}$. This is analogous to approximating a waveform with limited Taylor series terms, as shown in (7). The effect of neglecting the rest of the basis in a complete space is discussed.

Denote the neglected base vector as $\boldsymbol{k}_1$ (red arrow), then the accurate projection of vector $\boldsymbol{a}$ should be: $\boldsymbol{a} = \{\boldsymbol{i}, \boldsymbol{j}, \boldsymbol{k}_1\}\bullet(i_1, j_1, k_1)^{T}$. When least square is used, an orthogonal complementary vector of $\mathcal{S}$, denoted as $\boldsymbol{k}_2$, is assumed instead, and the resultant projection would be: $\boldsymbol{a} = \{\boldsymbol{i}, \boldsymbol{j}, \boldsymbol{k}_2\}\bullet(i_2, j_2, k_2)^{T}$. Besides the error from vector space truncation when forming H matrix, more errors are introduced when utilizing a non-orthogonal fitting vector space.

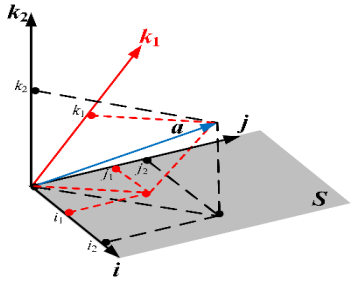

Figure 2. Illustration of Least Square Approximation Error

As a result, it is important to find a vector space whose complementary space is orthogonal to it, and has the same column space as H. This is effectively done by QR factorization, expressed in (15).

$$H = QR = [\hat{Q} : Q_2]\begin{bmatrix} \hat{R} \\ \boldsymbol{0} \end{bmatrix} \quad (15)$$

where matrix $\hat{Q}$ and H have the same column space, which is orthogonal to the column space of matrix Q_2, and $Q^{-1}=Q^{T}$. From this point, matrix $\hat{Q}$ will be used instead of H.

Rewrite (14), since

$$x(\boldsymbol{t}) = H\boldsymbol{d} = [\hat{Q}, Q_2]\begin{bmatrix}\hat{R}\\ \mathbf{0}\end{bmatrix}\boldsymbol{d} = [\hat{Q}, Q_2]\begin{bmatrix}\hat{R}\boldsymbol{d}\\ \mathbf{0}\end{bmatrix} \quad (15)$$

Therefore,

$$\begin{bmatrix}\hat{R}\boldsymbol{d}\\ \mathbf{0}\end{bmatrix} = ([\hat{Q}, Q_2])^{-1}x(\boldsymbol{t}) = ([\hat{Q}, Q_2])^{T}x(\boldsymbol{t}) = \begin{bmatrix}\hat{Q}^T\\ Q_2^T\end{bmatrix}x(\boldsymbol{t}) \quad (16)$$

Neglecting orthogonal complementary subspace Q_2, and re-write (14):

$$\hat{R}\boldsymbol{d} = \hat{Q}^T x(\boldsymbol{t}) = \hat{Q}^T M\boldsymbol{c} \quad (17)$$

Note that vector $\boldsymbol{d}$ is implicit, and does not need to be calculated. By utilizing QR factorization of fitting matrix H, extra approximation error from least square calculation is avoided.

IV. Implementation and Simulation Analysis

A. Algorithm Implementation

In order to improve estimation accuracy, an observation window longer than one cycle is used. The whole observation window is further truncated into several overlapping windows each with the length of one cycle. The number of overlapping windows depends on the number of terms of approximation. To balance the known and unknown parameters in (8), at least three overlapping windows with selected hop size should be used. The assumption is that in the span of few extra samples, the signal features for waveforms and harmonics will not change, which is reasonable for electromechanical dynamics given the large inertia of the electric generators.

In this test, three overlapping window with length of one cycle and hop size of 5 samples are used, resulting in a total observation window of one cycle plus 10 samples. Note that for each observation window, matrix H will change slightly since the expansion is w.r.t to the center of window, according to (8).

With this configuration, (11) and (17) can be rewritten as (18) and (19), respectively, and the final implementation scheme is shown in Fig. 3.

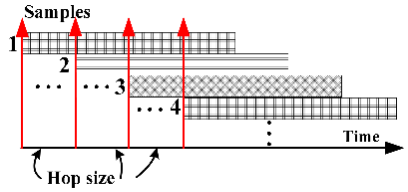

Figure 3. Illustration of Overlapping Windows and Hop Size

$$\begin{bmatrix}AH_1\\ AH_2\\ AH_3\end{bmatrix}\boldsymbol{c} = A\begin{bmatrix}x_1(\boldsymbol{t})\\ x_2(\boldsymbol{t})\\ x_3(\boldsymbol{t})\end{bmatrix} \quad (18)$$

$$\begin{bmatrix}\widehat{Q_1}^T M\\ \widehat{Q_2}^T M\\ \widehat{Q_2}^T M\end{bmatrix}\boldsymbol{c} = \begin{bmatrix}\widehat{Q_1}^T x_1(\boldsymbol{t})\\ \widehat{Q_2}^T x_2(\boldsymbol{t})\\ \widehat{Q_3}^T x_3(\boldsymbol{t})\end{bmatrix} \quad (19)$$

The final implementation procedures based on (18) and (19) are implemented in MATLAB for performance verification. The simulation results are shown in the following section.

It is worth pointing out that once vector $\boldsymbol{c}$ is obtained, the original time domain waveform may be reconstructed using the model in Algorithm B.

B. MATLAB Simulation Results and Evaluation

Fourier method and monomial fitting method are used in the demonstration of algorithm hybridization framework. It is worth noting that since DFT and monomial methods respectively excel at eliminating harmonics, and modeling slow amplitude transients, the hybridized method in this experiment may not suit other types of waveforms, such as frequency ramping. The hybridization principle proposed in the paper can be applied to the concatenation of more algorithms. In this test, waveforms containing both harmonics and slow amplitude transients are used as test waveforms. The sampling frequency is 6kHz, and hop size is 5 samples. Since data window length is one cycle plus 10 samples. 10% harmonic level is used. The magnitude errors shown are normalized.

1) Accuracy Evaluation Criteria

In most cases, phasor parameters need to be calculated using vector $\boldsymbol{c}$. The complex domain quantities are usually associated with one single timestamp in an observation window, and a translation from phasor parameter calculation accuracy requirement to the requirement on signal parameter estimation is needed. Since waveform measurement magnitudes are the only parameter of interest from time domain waveforms, this paper only concerns with the magnitude error. Citing synchrophasor standards, the relative error requirement for waveform estimation at any time instant should be ten times higher than the TVE% requirement of synchrophasor, i.e. 0.1%.

2) Strategy 1: Monomial Fitting Method for Reconstruction:

In this case, slow transients are modeled directly while DFT is used to filter out harmonics. The results are shown in Table I.

TABLE I. Waveform Approximation Accuracy for Strategy 1

Largest Absolute Magnitude Error (%)	f_{AM} = 1Hz	f_{AM} = 2Hz	f_{AM} = 5Hz
2nd Harmonic	4.2×10^{-5}%	6.5×10^{-4}%	2×10^{-2}%
5th Harmonic	4.2×10^{-5}%	6.5×10^{-4}%	2×10^{-2}%
10th Harmonic	4.2×10^{-5}%	6.5×10^{-4}%	2×10^{-2}%
30th Harmonic	4.2×10^{-5}%	6.5×10^{-4}%	2×10^{-2}%
50th Harmonic	4.2×10^{-5}%	6.5×10^{-4}%	2×10^{-2}%

It can be observed that at a certain amplitude modulation frequency level, the accuracy is not affected by harmonic order, which is expected since the harmonic components are filtered out in the Fourier method. The estimation errors are only from curve fitting procedure. Adding more terms in (8) may improve the accuracy, but may also cause overfitting problem, which is not elaborated in this paper.

3) Strategy 2: Fourier Method for Reconstruction:

In this simulation, besides N DFT harmonic components, two extra frequencies, 55Hz, 65Hz, are added to model the sidebands from amplitude modulation. The slow varying transients are further modeled in six monomial terms shown in (14). The results are shown in Table II.

TABLE II. WAVEFORM APPROXIMATION ACCURACY FOR STRATEGY 2

Largest Absolute Magnitude Error (%)	2nd Harmonic	13th Harmonic	35th Harmonic
f_{AM} = 1Hz	1.6×10^{-2}%	5×10^{-3}%	5×10^{-3}%
f_{AM} = 2.3Hz	6×10^{-2}%	2×10^{-2}%	2×10^{-2}%
f_{AM} = 3.4Hz	0.1×10^{-2}%	2×10^{-2}%	2×10^{-2}%
f_{AM} = 4.5Hz	5×10^{-2}%	1×10^{-2}%	1×10^{-2}%
f_{AM} = 5Hz	0	0	0

Since harmonics are still completely filtered out, the estimation errors come from amplitude modulation sidebands. Because 55Hz and 65Hz only exactly model the sidebands at f_{AM} = 5Hz, estimation error cannot be completely eliminated otherwise. To alleviate the effect from sidebands, more frequencies in the vicinity of 60Hz can be potentially added in the Fourier model.

V. CONCLUSION

In this paper, a hybridization framework of existing phasor parameter calculation methods is proposed. The propose method offers a novel perspective of designing phasor parameter estimation algorithms by integrating the advantages of existing algorithms. The paper contributions are summarized as follows:

- To demonstrate the proposed hybridization rationale, Fourier method (DFT) and monomial fitting method are selected and hybridized.
- Two hybridization strategies are tested, depending on the algorithm chosen as the reconstruction algorithm. Both strategies are tested with theoretical mixed amplitude modulation and harmonics waveforms in MATLAB.
- The test results show that either proposed strategy is able to accurately approximate the original waveform by simultaneously suppressing harmonic components and modelling amplitude transients. The source of errors is analyzed.
- Theoretically, more algorithms can be concatenated and hybridized as long as the algorithms of interest can be written in a linear matrix formulation. Ultimately, the proposed framework dramatically reduces difficulty and improve the efficiency of algorithm design.

REFERENCES

[1]. Synchrophasor Applications in Transmission Systems. [Online]. Available: https://www.smartgrid.gov/recovery_act/program_impacts/applications_synchrophasor_technology.html

[2]. A. Silverstein and J. E. Dagle, "Successes and Challenges for Synchrophasor Technology: An Update from the North American SynchroPhasor Initiative," System Science (HICSS), 2012 45th Hawaii International Conference on, Maui, HI, 2012, pp. 2091-2095.

[3]. A. von Meier, D. Culler, A. McEachern and R. Arghandeh, "Micro-synchrophasors for distribution systems," Innovative Smart Grid Technologies Conference (ISGT), 2014 IEEE PES, Washington, DC, 2014, pp. 1-5

[4]. M. Wache and D. C. Murray, "Application of Synchrophasor Measurements for distribution networks," Power and Energy Society General Meeting, 2011 IEEE, San Diego, CA, 2011, pp. 1-4.

[5]. G. Hataway, B. Flerhinger, R. Moxley, Synchrophasors for Distribution Applications. [Online]. Available: https://cdn.selinc.com/assets/Literature/Publications/Technical%20Papers/6561_ SynchrophasorsDistribution_RM_20121030_Web.pdf

[6]. A. von Meier, D. Culler, A. McEachern and R. Arghandeh, Micro-synchrophasors for distribution systems, Innovative Smart Grid Technologies Conference (ISGT), 2014 IEEE PES, Washington, DC, 2014, pp. 1-5. [Online]. Available: http://arxiv.org/abs/1408.1736

[7]. A. von Meier, R. Arghandeh, Every Moment Counts: Synchrophasors for Distribution Networks with Variable Resources. [Online]. Available: http://arxiv.org/ftp/arxiv/papers/1408/1408.1736.pdf

[8]. J. A. de la O Serna, "Dynamic Phasor Estimates for Power System Oscillations," in IEEE Transactions on Instrumentation and Measurement, vol. 56, no. 5, pp. 1648-1657, Oct. 2007.

[9]. IEEE Standard for Synchrophasor Measurements for Power Systems -- Amendment 1: Modification of Selected Performance Requirements," in IEEE Std C37.118.1a-2014 (Amendment to IEEE Std C37.118.1-2011) , vol., no., pp.1-25, April 30 2014.

[10]. A. Phadke, J. Thorp, Synchronized Phasor Measurements and Their Applications, Springer Science+Business Media, LLC, 2008.

[11]. T. Bi, H. Liu, Q. Feng, C. Qian, and Y. Liu, "Dynamic Phasor Model-Based Synchrophasor Estimation Algorithm for M-Class PMU," IEEE Trans. Power Delivery, vol.30, no.3, pp.1162-1171, June 2015.M. Klein, G. J. Rogers and P. Kundur, "A fundamental study of inter-area oscillations in power systems," in IEEE Transactions on Power Systems, vol. 6, no. 3, pp. 914-921, Aug 1991.

[12]. C. Qian, M. Kezunovic, "Spectral Interpolation for Frequency Measurement at Off-Nominal Frequencies," 2017 IEEE PES General Meeting, Chicago, IL, 2017, pp. 1-5

[13]. P. Romano and M. Paolone, "Enhanced Interpolated-DFT for Synchrophasor Estimation in FPGAs: Theory, Implementation, and Validation of a PMU Prototype," in IEEE Transactions on Instrumentation and Measurement, vol. 63, no. 12, pp. 2824-2836, Dec. 2014.

[14]. W. Premerlani, B. Kasztenny and M. Adamiak, "Development and Implementation of a Synchrophasor Estimator Capable of Measurements Under Dynamic Conditions," in IEEE Transactions on Power Delivery, vol. 23, no. 1, pp. 109-123, Jan. 2008.C. Qian, M. Kezunovic, "Dynamic Synchrophasor Estimation with Modified Hybrid Method," 2016 IEEE PES ISGT Conference, Minneapolis, MN, USA, 2016, pp. 1-5.

[15]. C. Qian, T. Bi, J. Li, H. Liu and Z. Liu, "Synchrophasor estimation algorithm using Legendre polynomials," 2014 IEEE PES General Meeting | Conference & Exposition, National Harbor, MD, 2014, pp. 1-5.

[16]. M. A. Platas-Garza and J. A. de la O Serna, "Dynamic Harmonic Analysis Through Taylor–Fourier Transform," in IEEE Transactions on Instrumentation and Measurement, vol. 60, no. 3, pp. 804-813, March 2011.

[17]. M. Bertocco, G. Frigo, C. Narduzzi, C. Muscas and P. A. Pegoraro, "Compressive Sensing of a Tay-lor-Fourier Multifrequency Model for Synchrophasor Estimation," in IEEE Transactions on Instru-mentation and Measurement, vol. 64, no. 12, pp. 3274-3283, Dec. 2015.

[18]. D. Belega, D. Fontanelli and D. Petri, "Low-Complexity Least-Squares Dynamic Synchrophasor Esti-mation Based on the Discrete Fourier Transform," in IEEE Transactions on Instrumentation and Measurement, vol. 64, no. 12, pp. 3284-3296, Dec. 2015.